

CRYOGENIC THERMAL DESIGN OF SMALL ELECTROMAGNETIC FORMATION FLIGHT SATELLITES

Daniel W. Kwon
Massachusetts Institute of Technology
Department of Aeronautics and Astronautics
77 Massachusetts Ave, Room 37-344a, Cambridge, MA 02139
dankwon@mit.edu
Advisor: Raymond J. Sedwick

ABSTRACT

Electromagnetic Formation Flight (EMFF) is a novel propellantless propulsion technology for formation flying satellites. Actuation in relative degrees of freedom for formation flight satellites is provided using electromagnetic forces and reaction wheels. One application for EMFF is stationkeeping for fractionated spacecraft architectures. The benefit of EMFF is that by replacing thrusters for formation flying actuation, a system is no longer reliant on consumables. Since the amount of fuel onboard small formation flying satellites can be limiting, EMFF can enable high ΔV formation flying missions for small satellites. EMFF is implemented by creating a steerable electromagnetic dipole using three orthogonal electromagnetic coils made of high temperature superconducting wire. One of the challenges of EMFF is that the superconducting wire requires a cryogenic thermal control system. This paper describes a consumable-free cryogenic thermal control system for EMFF. A cryogenic heat pipe is used to maintain cold temperatures throughout the superconducting coil while a cryocooler is used to extract heat. The design, build, and test of the cryogenic heat pipe used for superconductor cooling are presented in this paper.

INTRODUCTION

One of the challenges to small formation flying spacecraft is that the mission lifetime can be limited by consumables. A propellantless propulsion concept called Electromagnetic Formation Flight has been developed at MIT and the University of Maryland, which can be used to extend mission lifetime for small satellite systems. Forces and Torques are created by electromagnetic coils made of high temperature superconducting (HTS) wire. With a reaction wheel, one can de-couple the forces and torques and provide all necessary actuation in relative degrees of freedom. EMFF has application for stationkeeping distributed space satellites, such as a fractionated spacecraft architecture [1] and for space interferometry missions [2]. Another application of EMFF is using the

electromagnetic coil as a torque coil for angular momentum management.

Superconducting wire is an enabling technology for EMFF because it allows the creation of a large dipole field. One of the challenges of using superconducting wire is that it requires a low temperature for operation. The critical temperature for commercial off the shelf (COTS) HTS wire from American Superconductor is 110 K [3]. A key design characteristic of the EMFF thermal control system is that it must also be a consumable-free system. The main components of the thermal system include a cryocooler for heat extraction and a cryogenic heat pipe to maintain cryogenic temperatures throughout the coil. One benefit of these various cryogenic cooling technologies is that they have been demonstrated in space. Sunpower Inc. has flown their M77 cryocooler on the RHESSI mission in 2002 and Ball Aerospace flew a Joule-Thomson cryocooler on STS-85 in 1997 [4]. Also demonstrated on the shuttle was a cryogenic heat pipe (CRYOHP) on STS-53 in 1992, which operated between 60 to 140 K [5]. Heat pipes have also been used within a solar array, connecting opposite faces of the solar array; one side of the heat pipe is located on the cell side facing the sun, while the other end is connected to the radiators. Because of their flight heritage, cryocoolers and cryogenic heat pipes are promising technologies for the EMFF thermal system.

Another challenge of keeping the EMFF coils at cryogenic temperatures is the constantly changing heating environment around Earth orbit. Because of the rapidly changing orientation of the vehicles and the presence of constant heat from the Earth and sun, sun shields are not practical for EMFF. The challenge of cooling space structures, such as the EMFF coils, using self-sufficient active cooling is a unique problem.

Development of an EMFF ground testbed by the MIT Space Systems Laboratory started in 2002 by an undergraduate design and build course. Two EMFF testbed vehicles were built, each with two coils allowing for a steerable dipole in two dimensions. The design for the testbed thermal system used a bath of

liquid nitrogen to cool the HTS wire. Past work on the thermal system determined that a cryocooler was necessary for heat extraction on-orbit and COTS cryocoolers had the ability to extract the tens of watts necessary for steady state cooling [2]. In addition, a comparison of insulation systems consisting of a vacuum gap or aerogel was conducted in both LEO and in Earth-trailing orbit, which is outside of the Earth's heating environment. Other research on EMFF has investigated the dynamics and control for EMFF spacecraft in deep space and low Earth orbit and closed loop control experiments on the EMFF testbed [6].

DESIGN OVERVIEW

An overview of the EMFF cryogenic thermal control system is shown in Figure 1. Shown is a single HTS coil for testing inside a vacuum chamber. The HTS wire is shown as a block of wire wrapped around a thermally conductive jacket. The function of the thermal jacket is to maintain circumferential isothermalization of the HTS coil. It is also used to provide structure for the HTS wire stack and for electrical isolation. Around the thermal jacket is multilayer insulation, which reduces the heat load into the coil. The cryocooler is attached to the thermally conductive jacket and is used for heat extraction.

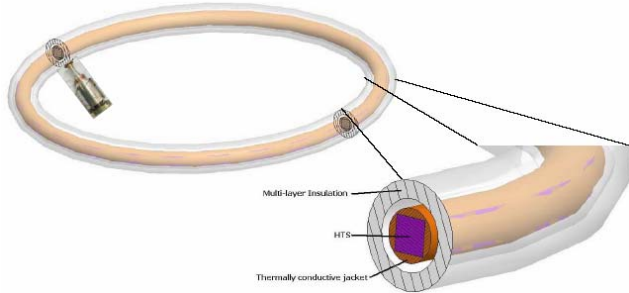


Figure 1 EMFF thermal system design

Previous work has been done modeling the thermally conductive jacket as a solid conductor [7]. Experimental testing of the system was also performed using liquid nitrogen in place of a cryocooler for heat extraction. A limitation of using a solid conductor is that the thermal conductivity of the material is not sufficient to maintain temperatures below the critical temperature. Therefore, it was proposed to use a heat pipe as the thermal jacket.

HEAT PIPE MODELING

Heat pipes work using two phase flow properties of a working fluid and in doing so can act like a material with very high thermal conductivity. There are typically three operating regions within a heat pipe, the condenser, evaporator, and an adiabatic region, which

are shown in Figure 2A. Power input into the evaporator causes the working fluid to evaporate. The vapor then flows to the condenser region where it is deposited and power flows out of the heat pipe. Capillary action in the wicking layer, where the liquid resides, pumps the liquid from the condenser to the evaporator. In order for circulation of the liquid and gas in the heat pipe, the capillary pressure drop must overcome the sum of pressure drops in the liquid and vapor phase plus any gravitational head.

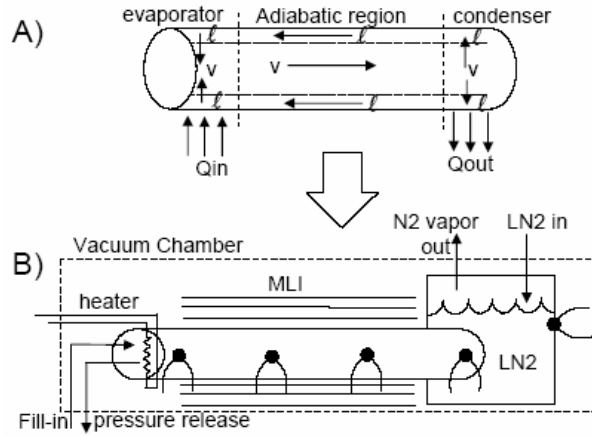


Figure 2 A) Heat pipe regions B) Experimental setup

The standard pressure balance equation for a heat pipe is therefore given by

$$\Delta P_c = \Delta P_v + \Delta P_l + \Delta P_g \quad (1)$$

The maximum capillary head, ΔP_c , is given by

$$\Delta P_c = \frac{2\sigma}{r_c} \cos \theta \quad (2)$$

where σ is the liquid surface tension and r_c is the pore radius of the mesh used for the wicking layer. The angle θ is the contact angle and $\theta = 0^\circ$ for a perfectly wetting liquid. The liquid pressure drop, ΔP_l , is given by Darcy's law [8] for flow through porous media

$$\Delta P_l = \frac{\mu_l L_{eff} \dot{m}}{\kappa \rho_l A_w} \quad (3)$$

where μ_l is the liquid viscosity, ρ_l is the liquid density, \dot{m} is the liquid flow rate, and A_w is the cross-sectional area of the wick. The effective length of the heat pipe, L_{eff} , is the distance from the center of the condenser to the center of the evaporator. The permeability of the wick, κ , is a function of the wick type, wick effective pore radius, permeability, and porosity. Empirical values for κ have been calculated for commonly used wick structures [9]. The gravitational pressure head, ΔP_g , depends on the relative elevations of the evaporator and condenser and is zero for a horizontal heat pipe. The vapor pressure drop, ΔP_v , is usually

much smaller than the liquid pressure drop and for initial calculations can be neglected.

For a horizontal heat pipe with a perfectly wetting liquid and ignoring the vapor pressure drop, Eq. (1) becomes

$$\frac{2\sigma}{r_c} = \frac{\mu_l L_{eff} \dot{m}}{\kappa \rho_l A_w} \quad (4)$$

Substituting $Q_{max} = \dot{m}_{max} h_{fg}$, where h_{fg} is the latent heat of vaporization for the working fluid, and solving for Q_{max} , the maximum power capacity of the heat pipe is given by

$$Q_{max} = \frac{2\sigma}{r_c} \frac{\kappa \rho_l A_w h_{fg}}{\mu_l L_{eff}} = 2 \left(\frac{\rho_l \sigma h_{fg}}{\mu_l} \right) \left(\frac{A_w}{L_{eff}} \right) \left(\frac{\kappa}{r_c} \right) \quad (5)$$

The first quantity in Eq. (5) is known as the figure of merit, M , for a working fluid. The figure of merit is a function of the fluid properties and varies as a function of temperature. A working fluid has a given range of temperature over which it performs favorably and each fluid has an optimum operating temperature. The higher the merit number, the better the fluid performs. The second quantity in Eq. (5) contains design parameters of the heat pipe. Characteristics of the wicking structure are in the third quantity. Technically, the wick area is also a function of the number of layers of wick and wick type used, but the main driving component is the diameter of the pipe. The wick area for a screen mesh is given by

$$A_w = 2\pi d d_w N \quad (6)$$

where N is the number of layers of screen mesh, d is the pipe diameter and d_w is the diameter of the wire mesh. The factor of two accounts for overlapping wires in the mesh. Since a heat pipe is operating at or near the saturation temperature of a working fluid, there are a few suitable options including, nitrogen, ammonia, and oxygen. Nitrogen is a suitable working fluid because of its ease of use when compared to the other options. The figure of merit for nitrogen is $9.1 \cdot 10^9$ W/m² for saturation conditions at 77 K, 1 atm.

The design goal for the heat pipe is to have a capacity of at least 5 Watts, if operating in space [2]. For this paper, we plan to build and test a heat pipe that is applicable to small satellites and can also fit inside an available vacuum chamber. The vacuum chamber has a 60 cm diameter and is 1 m long. Therefore, the length of a straight pipe is constrained to less than 1 meter. For simplicity, a straight heat pipe was constructed. A toroidal heat pipe for small satellites, which can be tested inside the vacuum chamber would have a similar condenser to evaporator length, so testing of a straight

~1 m heat pipe is a representative system. The radiation from the chamber walls provides a heating environment of approximately 30 Watts. In order to test a range of operating input powers, a heat pipe with a total power capacity of approximately 50 Watts has been investigated. The dimensions of the heat pipe should be large enough to contain a stack of HTS wire and be long enough to demonstrate that a flight sized coil could be cooled with a few connected heat pipes. Since a cryocooler will be used on the condenser end to extract power, the number of heat pipes in the system determines the number of cryocoolers necessary. The height of a single stack of HTS wires with 33 turns in the EMFF testbed is 1.32 cm. For a 100 turn stack, the total height is 4 cm, which fits within a 1.5 inch diameter pipe. The heat pipe envelope material is copper, which is selected since it has a high thermal conductivity and simplifies manufacturing procedures. Also for ease of construction stainless steel mesh is chosen as the wicking structure.

SINGLE SCREEN MESH DESIGN

Using Eq. (5), the heat pipe power capacity for a 100 and 250 wire mesh as a function of the pipe diameter, d , is shown in Figure 3. Four layers of the wrapped screen were used. Power increases linearly as a function of diameter because as the pipe diameter increases the flow area for the liquid also increases allowing for more heat to be pumped through the pipe. The heat capacity will also increase with additional layers of screen since the flow area increases. The results in Figure 3 are for a 1 m length pipe with a diameter that can accommodate an HTS stack between 33 turns ($d = 15$ mm) and 100 turns ($d = 40$ mm). However, the design of a heat pipe using a single type of screen mesh has insufficient power capacity.

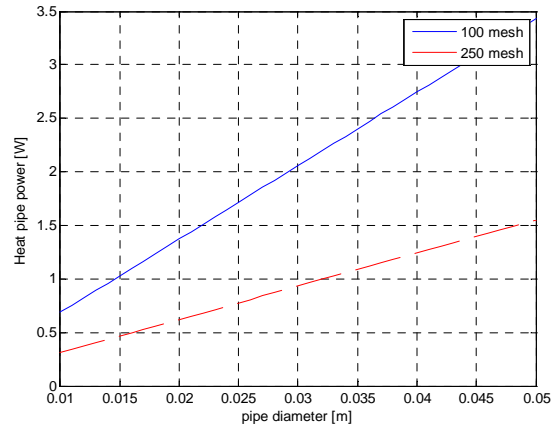


Figure 3 Heat Pipe power vs. pipe diameter for 100 and 250 wire mesh screens, each with 4 layers

Figure 3 indicates that a lower mesh number is favorable, however there is an interesting trade off that exists for screen meshes. A lower mesh number has a higher permeability, κ , which allows for liquid to travel from the condenser to the evaporator more easily. The trade off is that lower mesh numbers also have a larger pore radius. With respect to capillary pressure, a smaller pore radius is more favorable. Therefore, the ratio of permeability to pore radius is a key quantity in Eq. (5), which varies with mesh number.

MULTIPLE SCREEN MESH DESIGN

In order to obtain the small pore benefits of fine screen meshes and the high permeability benefits of coarse screen meshes, two different mesh types are investigated. For this analysis, two layers of a 100 mesh screen and two layers of a 250 mesh screen are used. The coarse mesh is located in between the copper wall and the fine mesh. The fine mesh acts to hold the liquid in the wick structure and provides the capillary pumping pressure. The coarse mesh allows for the liquid to travel with ease to the evaporator. The results for this design are shown in Figure 4. For a 100 turn HTS stack, requiring a 40 mm pipe diameter, the power of the heat pipe is approximately 10 Watts, which is sufficient for a space heat pipe design. This is approximately a three-fold improvement over a design using just a 250 mesh screen with 4 layers.

Since using a more coarse mesh is favorable, the power for a heat pipe using a 30 mesh inner layer is shown in Figure 5 by the red dashed line. A heat pipe with the 30 mesh inner layer shows large improvements over the 100 inner mesh design. Therefore using multiple mesh numbers allows the heat pipe to achieve a performance that meets our requirements.

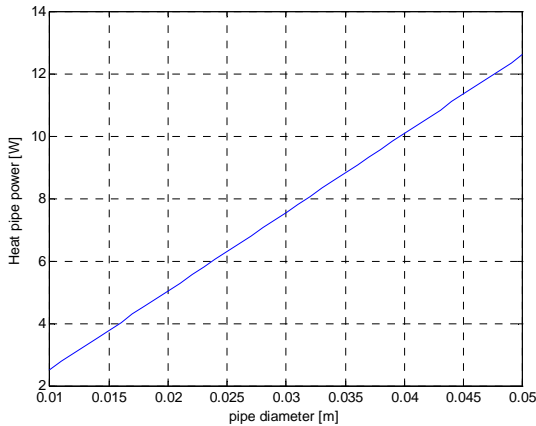


Figure 4 Heat pipe design for a 100 inner mesh, 250 outer mesh (2 layers each), 1 m pipe.

In order to achieve a power capacity of approximately 50 Watts, a 50 mesh number inner layer was used. Table 1 summarizes the parameters of the heat pipe design.

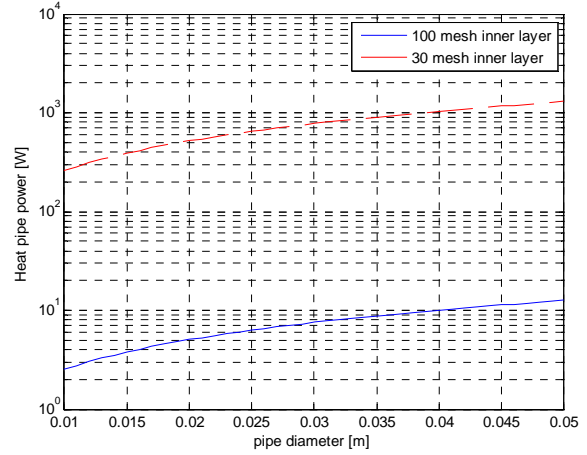


Figure 5 Heat pipe designs using 30 or 100 inner mesh layer, 250 outer mesh

Table 1 Heat pipe specifications

Heat pipe length	85.5 cm
Pipe diameter	40 mm
Wick material	Stainless steel mesh
Inner mesh layers	2 layers of 50 mesh
Outer mesh layers	2 layers of 250 mesh
Condenser length	6 cm
Condenser temperature	~77 K (liquid nitrogen)
Working fluid	Nitrogen
Envelope material	Copper
Power capacity	55 W

TEMPERATURE MODELING

Since the performance of the superconducting wire is limited by the section of wire that is hottest, it is important to estimate the temperature of the heat pipe that is farthest away from the condenser. This hot end temperature is T_e , the temperature at the evaporator. A resistive network can be used to model the heat pipe and is shown in Figure 6. The total temperature drop from the evaporator to the condenser, ΔT , can be solved from

$$Q = \frac{\Delta T}{R_t} \quad (7)$$

where R_t is the total thermal resistance of the heat pipe. In terms of the condenser temperature and evaporator temperature, Eq. (7) can be solved for the evaporator temperature on the pipe as

$$T_e = \frac{Q}{U_{HP,p}A} + T_c \quad (8)$$

where A is the thermal resistances based on the pipe cross-sectional area (πr_o^2), and the sum of the thermal resistances are simplified as

$$U_{HP,p} = \frac{1}{R_{p,c} + R_{w,c} + R_{w,e} + R_{p,e}} \quad (9)$$

where $R_{p,c}$ and $R_{p,e}$ are the thermal resistances of the pipe wall in the condenser and evaporator respectively, and $R_{w,c}$ and $R_{w,e}$ are the thermal resistances of the wick in the condenser and evaporator respectively. These quantities are given by

$$\begin{aligned} R_{p,e} &= \frac{r_o t_p}{2L_e k_p} & R_{w,e} &= \frac{r_o^2 t_w}{2L_e r_i k_w} \\ R_{p,c} &= \frac{r_o t_p}{2L_c k_p} & R_{w,c} &= \frac{r_o^2 t_w}{2L_c r_i k_w} \end{aligned} \quad (10)$$

where r_o is the pipe outer radius, r_i is the pipe inner radius, t_p is the pipe wall thickness, L_e and L_c are the lengths of the evaporator and condenser, t_w is the wick thickness, k_p is the pipe wall thermal conductivity and k_w is the wick thermal conductivity. The conductivity of a wrapped screen [10] accounts for the liquid conductivity, k_l , the screen conductivity, k_s , the porosity of the mesh, ε , and is given by

$$k_w = k_l \frac{k_l + k_s - \varepsilon(k_l - k_s)}{k_l + k_s + \varepsilon(k_l - k_s)} \quad (11)$$

The thermal resistance of the wick accounts for both the coarse and fine mesh in series.

The system shown in Figure 6 simplifies the thermal resistance network because the resistance of the vapor space in the adiabatic region, $R_{v,a}$, is several orders of magnitude higher than the wick resistance [8]. Also the axial resistance of the wick and pipe was calculated to be approximately three orders of magnitude lower than the total calculated resistance.

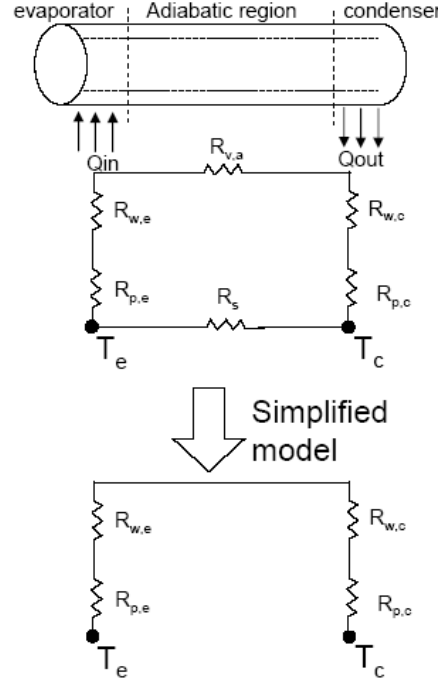


Figure 6 Heat pipe modeled as a resistive network

HEAT PIPE LIMITATIONS

There are some limitations to the heat pipe power capacity that are imposed by the working fluid and the design of the overall system. For a low temperature pipe, these limits are not expected to be a problem, however, each are investigated here for completeness.

Entrainment limit

Entrainment occurs when the vapor in the counter-current near the liquid-vapor interface is able to entrain liquid droplets. Qualitatively, this phenomenon occurs when the vapor is traveling at a fast enough velocity to create waves on the surface of the mesh. High velocity vapor occurs for heat pipes operating at large powers, since fast circulation of the working fluid is required. Thus the entrainment limit puts an upper bound on the power of a heat pipe. The equation for the entrainment limit [8] is given by

$$Q_{ent} = \pi r_v^2 h_{fg} \sqrt{\frac{2\pi\rho_v\sigma_l}{z}} \quad (12)$$

where z is the characteristic dimension of the liquid-vapor interface, ρ_v is the density of the vapor, and r_v is the radius of the vapor space. Reay [8] gives 0.036 mm as z , and for simplicity r_v is approximated as half the diameter of the heat pipe. For the heat pipe, the entrainment limit is 6.8 kW. Since $Q_{ent} \gg Q_{design}$ the entrainment limit is not a concern.

Sonic Limit

The sonic limit is the choking at the evaporator exit which limits the vapor flow through the heat pipe, thus putting a limit on the total power of the heat pipe. It is given by

$$Q_{sonic} = \frac{\pi}{4} d^2 \rho_v h_{fg} \sqrt{\frac{\gamma R T_v}{2(\gamma + 1)}} \quad (13)$$

where T_v is the temperature of the vapor, and R is the gas constant for nitrogen. For a heat pipe in steady state operation, T_v is simply the saturation temperature. For the heat pipe designed in Table 1, the sonic limit is calculated to be 12 kW. Again, the sonic limit is not a concern.

Vapor Core Diameter Limitations

A stack of HTS wires inside the vapor space has a second limitation unique to an EMFF heat pipe. The HTS wire stack reduces the vapor space and could potentially choke the flow. As a conservative estimate, the system is designed so that the vapor mach number is less than 0.2 for laminar and compressible flow.

$$M_v = \frac{Q}{\rho_v A_v h_{fg} \sqrt{\gamma_v R_v T_v}} < 0.2 \quad (14)$$

Accounting for the HTS stack, the area of the vapor space is now given by

$$A_v = \pi \frac{d_v^2}{4} - A_b \quad (15)$$

where A_b is the cross sectional area of the HTS wire stack. In terms of A_b , the sonic limit is given by

$$Q_{sonic} = 0.2 \rho_v h_{fg} \sqrt{\gamma_v R_v T_v} \left(\pi \frac{d_v^2}{4} - A_b \right) \quad (16)$$

For the heat pipe, the vapor flow blockage does not limit the system performance until the diameter of the blockage approaches the vapor space diameter. This result is shown in Figure 7. When the sonic limit is greater than the designed heat capacity, the heat pipe is still capillary limited.

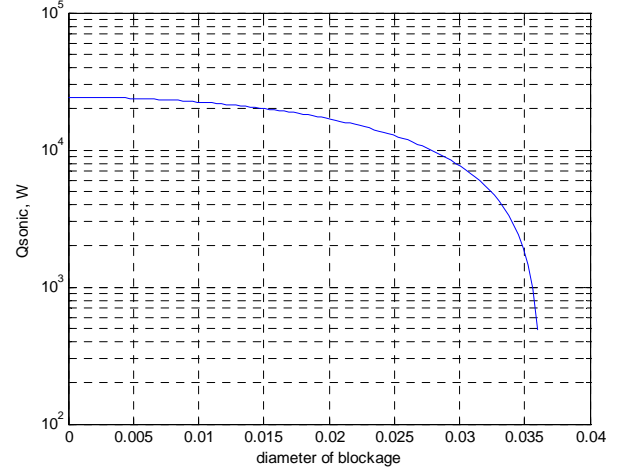


Figure 7 Vapor space limitations

HEAT PIPE IMPLEMENTATION

The cryogenic heat pipe is tested in a vacuum chamber in order to minimize convective heat exchange and to simulate an environment similar to space where radiation heating is the main heat source into the pipe. Figure 2 shows how the heat pipe is setup inside a vacuum chamber. A liquid nitrogen reservoir inside the chamber provides cooling for the condenser and mimics the function of a cryocooler. This reservoir is completely isolated from the heat pipe. While liquid nitrogen is in direct contact with the heat pipe, it does not enter the sealed pipe. Liquid nitrogen is brought into the reservoir via a vacuum chamber liquid feedthrough and any boiloff or excess liquid nitrogen is brought out of the chamber via a second feedthrough. At the other end of the heat pipe, a resistive heater is used to apply heat to the heat pipe. At this end is also a feed into the heat pipe to inject the working fluid. Using this same feed, the heat pipe is also connected to a pressure relief valve for safety. Multilayer insulation around the heat pipe can be used to create an adiabatic region, however for the experiment setup used, no MLI was applied. In fact, since there is radiation heating along the entire pipe, there is essentially no adiabatic region. Also shown are thermocouples which are applied throughout the heat pipe and on the liquid nitrogen reservoir.



Figure 8 Heat pipe and liquid Nitrogen reservoir

The heat pipe is shown in Figure 8. This picture shows the liquid nitrogen reservoir before it is soldered onto the heat pipe. The heat pipe condenser is 6 cm long and fits inside the reservoir opening shown. The copper bushing at 6 cm is then soldered onto the opening in the liquid nitrogen reservoir. The entire heat pipe assembly in the vacuum chamber is shown in Figure 9. There are fourteen thermocouples measuring the temperature of the heat pipe, liquid nitrogen reservoir, and vacuum chamber wall. Two G10 rods are used to support the heat pipe. There is also an electrical feedthrough used to power the resistive heater and to interface with the HTS wire.



Figure 9 Heat pipe in vacuum chamber

Figure 10 illustrates the devices that are connected to the heat pipe outside of the vacuum chamber. A relief valve and pressure gauge are directly connected to the vapor space of the heat pipe. The cryogenic relief valve is set at 35 PSIG. Before operating the heat pipe, the vapor space is evacuated using a lab vacuum pump to eliminate any non-condensable gases, which might block the condenser. Nitrogen gas is introduced at approximately 20 PSI and is measured using a flowmeter.

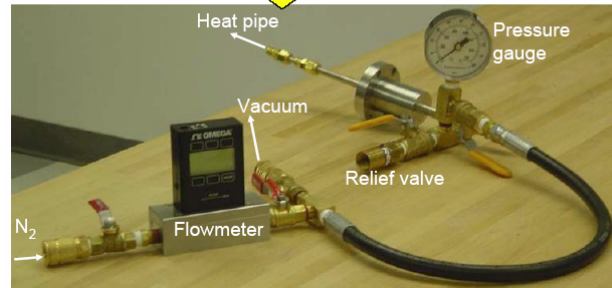
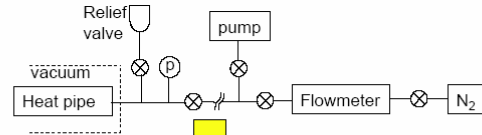


Figure 10 Working fluid injection setup

Heat Pipe Cleaning

Cleanliness of the working gas and the wick structure are important since it ensures wetting of the wick and removes particulates which can hinder the capillary action. Solid particulates can block the evaporator and in general plug the wick. Grease or other liquid contaminants affect working fluid wetting abilities and can reduce surface tension and viscosity, resulting in a reduction in the figure of merit for the working fluid. These issues are more critical for high temperature operation, especially for heat pipes using metal liquids, however the following steps were taken for the cryogenic heat pipe to remove particulates, degrease, and deoxidize contaminants [11].

Steps to clean the copper envelope

1. Soak and rinse the tube with an acetone solution to remove oils and grease.
2. Soak in an acid bath of 50% phosphoric acid and 50% nitric acid for 15 minutes. The acid pickle is used to remove oxidation from the copper and also clean it from oils and grease.
3. System is rinsed with water, then air dried.

Steps to clean the stainless steel mesh

1. Soak and rinse the tube with an acetone solution to remove oils and grease.
2. Soak in an acid bath of 80% distilled water, 15% nitric acid and 5% Hydrochloric acid for 15 minutes.
3. Soak in an acid bath of 85% distilled water and 15% nitric acid for 15 minutes.
4. System is rinsed with water, then air dried.

To test for good cleanliness and a good wetting surface, a drop of demineralized water is applied to the cleaned surface. If the drop spreads immediate on the copper or

is absorbed completely into the wick, the system has been properly cleaned. It is important to note that all cleaning procedures and handling of the heat pipe is conducted with gloves because even grease from hands can contaminate the system. Similar to the theme of cleanliness, a working fluid that is highly pure is important. Low temperature fluids need to avoid the presence of water to prevent any incompatibilities.

HTS wire insertion

Since the straight heat pipe is unable to test a coil of HTS wire, two straight HTS wire pieces were inserted into the pipe and connected at one end. Figure 11 shows the connectors to the HTS wire on the outside of the sealed pipe. It also shows the resistor, which is screwed onto a curved piece of copper, which is soldered onto the heat pipe.

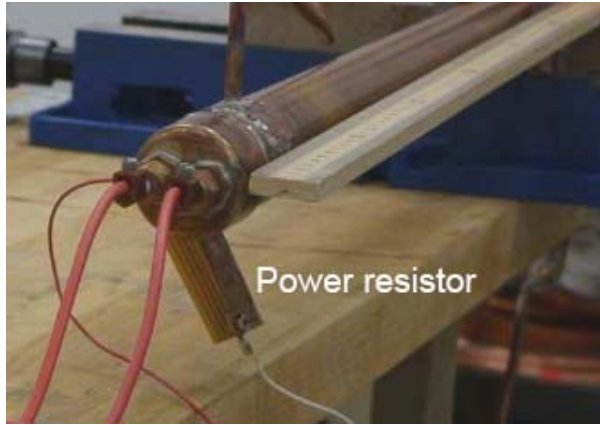


Figure 11 Power resistor and HTS wire connectors on the heat pipe

A coil of HTS wire in an EMFF spacecraft contains over a hundred turns of wire. This entire amount of wire must be cooled down before the coils can operate at superconducting levels. In addition, the wire stack could choke the vapor space, if it were sufficiently large. In order to mimic the thermal mass and the potential vapor blocking effect, a circular aluminum block was also inserted into the heat pipe. A groove was machined into the aluminum so that the two HTS wires would be press fit inside the block. Since the center of the block is likely the last portion of the aluminum to cool down, the HTS wires are placed close to the center. This gives a good indication for how long it might take an entire stack of wires to cool down.



Figure 12 Heat pipe with aluminum block and HTS wire

A wheatstone bridge is used to determine the drop in resistance for the HTS wire during heat pipe operation and is shown in Figure 13. One leg of the wheatstone bridge is the superconducting wire, while the other three legs are known resistances. The voltage of the bridge is given by

$$V_g = \left(\frac{R_x}{R_3 + R_x} - \frac{R_2}{R_1 + R_2} \right) V_d \quad (17)$$

where R_x is the superconductor, and the values for R_1 , R_2 , and R_3 are shown in Figure 13. To determine the resistance of the superconductor, Eq (17) is solved for R_x and is given by

$$R_x = \frac{R_3 \left(R_2 + \frac{V_g}{V_d} (R_1 + R_2) \right)}{R_1 - \frac{V_g}{V_d} (R_1 + R_2)} \quad (18)$$

In order to determine the change in resistance for the HTS from non-superconducting to superconducting state, a 21 cm diameter, 21 turn coil was dunked into liquid nitrogen. Its change in resistance was measured, and the resistance per meter was found to be approximately 40 mΩ/m. The length of the HTS wire in the heat pipe is approximately 1.64 meters long, so the expected drop in resistance is approximately 65 mΩ.

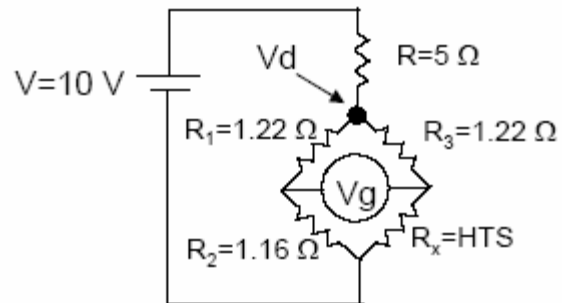


Figure 13 Wheatstone bridge circuit

EXPERIMENTAL RESULTS

Heat Pipe Tests

The heat pipe was first tested without the aluminum block and HTS wire to verify the power capacity and thermal resistance models. The temperature profile as a function of time for the heat pipe is shown in Figure 14. Initially the heat pipe is at room temperature. At zero minutes, liquid nitrogen is flowed into the liquid nitrogen reservoir. The temperature at the middle of the reservoir, denoted by a solid cyan line (ResBot), is the first thermocouple to drop in temperature. There are five thermocouple pairs located at various distances away from the condenser. The first pair (red) is right next to the condenser, on the opposite side of the copper bushing which is soldered to the reservoir. This location is the '0' origin measuring the axial distance away from the condenser. The other thermocouples are located at 10 cm (blue), 25 cm (green), 50 cm (black), and 75 cm (magenta) away from the condenser. For each pair of thermocouples, one thermocouple is located on the bottom of the pipe, indicated by a solid colored line, and the other is on the top of the pipe, indicated by the dashed line. In addition, the wall temperature of the vacuum chamber is shown in yellow.

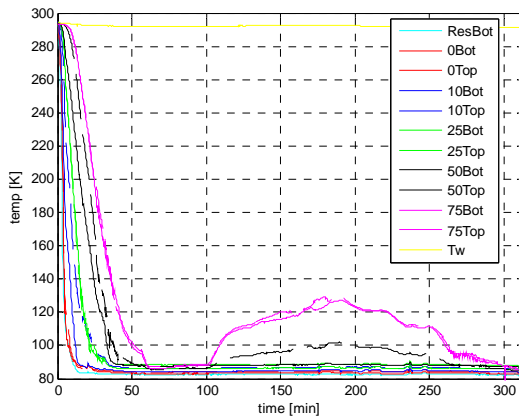


Figure 14 Heat pipe operation

Working fluid is added to the heat pipe as the pipe temperature drops until the wick is fully wet. Once this occurs, the temperature across the pipe is relatively isothermal. For the test shown in Figure 14, the heat pipe reaches saturation conditions after approximately 60 minutes. To test when dry-out of the wick occurs, heat is added to the system using the power resistor at the end of the pipe. The resistor power profile is shown in Figure 15. The temperature of the heat pipe is allowed to reach an approximate steady state after 30 minutes at each power level. After power was applied, the heat pipe was returned back to steady-state saturation conditions.

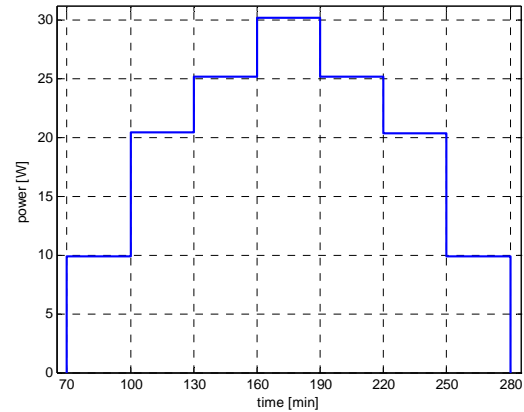


Figure 15 Power into heat pipe from resistor

Dry-out of the wick occurs somewhere between 25 and 30 Watts of applied power. The power coming into the pipe from the chamber radiation environment is approximately 30 Watts. So the measured total power capacity of approximately 55 to 60 Watts is close the designed power capacity of approximately 50 Watts. These differences can come from how dry-out is interpreted from the temperature data.

Using the data from Figure 14 and other tests, a comparison of the evaporator temperature as a function of total power into the pipe is shown in Figure 16. It is important to note that the resistive network model only accounts for the heat pipe in steady-state operation. Dry-out is not captured by the model, which is why there is difference for regions of high power into the heat pipe. The model shows good correlation around the designed steady-state power operation of approximately 50 Watts.

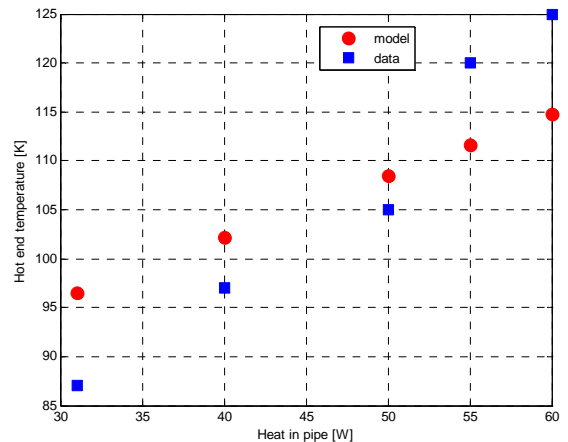


Figure 16 Temperature at end vs. total power input

Tests with HTS wire

After verifying operation of the cryogenic heat pipe, the HTS wire and aluminum block were inserted and tested. The temperature profile for the heat pipe is shown in Figure 17. One extra pair of thermocouples was added to the heat pipe and some of the thermocouples were moved to have greater concentration at the hot end, farthest away from the condenser. Pairs of thermocouples are located at 0 cm (black), 25 cm (green), 50 cm (red), 65 cm (blue), 70 cm (magenta), and 75 cm (cyan) away from the condenser. The wall temperature and liquid nitrogen reservoir temperatures are also shown in yellow.

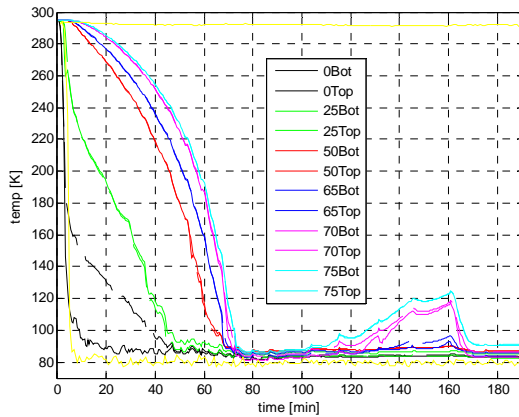


Figure 17 Test of Heat Pipe with HTS wire

The same procedure of filling the heat pipe was used with working fluid injected at periodic intervals. With the HTS wire tests, it was noticed that the heat pipe took a longer time to cool down and working fluid needed to be injected at more intervals. The cumulative working fluid mass in the heat pipe is shown in Figure 18. The steady-state working fluid mass needed to fully wet the wick is approximately 65 g. During testing it was observed that the heat pipe was leaking some working fluid into the vacuum chamber at a rate of approximately 3.1 g every 10 minutes. To compensate for this, additional working fluid was injected occasionally. An example of this is seen by additions to the working fluid cumulative mass at approximately 105 and 115 minutes into testing. After a test is conducted the working fluid is evacuated from the heat pipe and measured. For the test shown in Figure 17, working fluid was evacuated at 190 minutes. The leak in the heat pipe also accounts for the difference in final working fluid mass seen in Figure 18

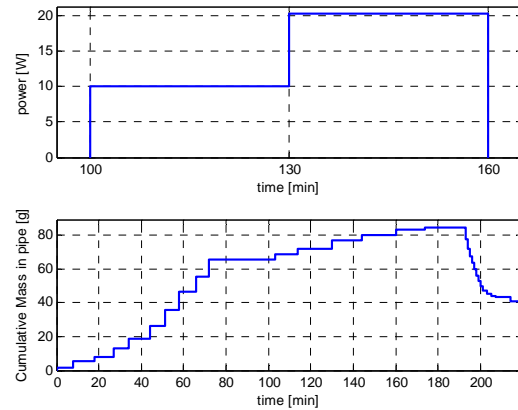


Figure 18 Power from Resistive Heater and Working Fluid Mass Injected

The test shown in Figure 17 achieved saturation conditions throughout the heat pipe at approximately 75 minutes. After 25 minutes of steady-state operation, the power resistor was turned on to 10 Watts. The power profile of the resistor is shown in Figure 18. For this test, a maximum of 20 Watts was applied before dry-out occurred. This is close to the same conditions that dry-out occurred in the pipe without the aluminum block and HTS wire. During these tests, when the HTS wire is on, but not yet superconducting, the vapor space is heated. In addition, working fluid leaking out of the pipe causes the wick to dry-out faster than before.

The resistance of the HTS wire during the test can be determined from the wheatstone bridge. The drop in resistance is shown in Figure 19. The solid line shows the approximate baseline resistance of the wire connections that are non-superconducting. At approximately 75 minutes, when the heat pipe is at saturation conditions, the entire HTS wire is in a superconducting state. It appears that the superconductor is also operating at superconducting levels even when dry-out occurs. From Figure 17, temperatures measured on the outside of the heat pipe are above the critical temperature (110 K), however it is likely that the current wheatstone bridge is not sensitive enough to detect small portions of change in superconductor resistance which occur on the order of a few centimeters of the HTS wire. The overall results of testing shows that the HTS wire can be cooled in the vapor space of a cryogenic heat pipe.

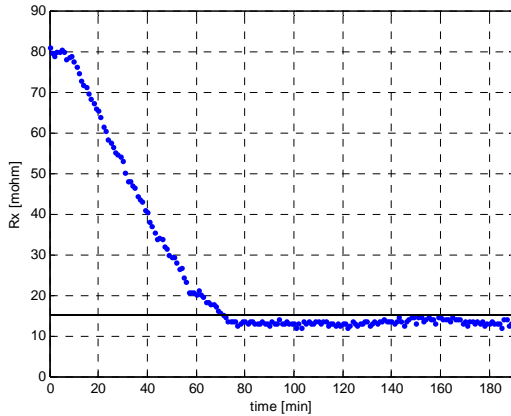


Figure 19 HTS change in resistance

CONCLUSIONS

A unique propellant-less propulsion concept for formation flight satellites is Electromagnetic Formation Flight. EMFF has the potential to enable new types of missions for small satellites, that before, might have been limited by consumables. To utilize EMFF, a cryogenic thermal control system is needed to cool the high temperature superconducting coils. To maintain uniform temperatures a cryogenic heat pipe is used with the HTS wires inside the vapor space. Nitrogen gas was used as a working fluid with a stainless steel mesh as a wicking structure. Design of a wick with multiple layers of fine and coarse mesh was shown to transport enough heat to allow for saturation conditions throughout the entire pipe length. As a proof of concept, a capillary limited heat pipe was designed for testing in a vacuum chamber. A straight heat pipe was tested first without the HTS wires to verify the power capacity of the heat pipe and the temperature at the evaporator. Tests were also conducted with HTS wires and used an aluminum block to act as the thermal mass and potential choking obstacle that a large number of HTS wires might present. Using a wheatstone bridge, it was found that the HTS wires achieved a superconducting state during steady-state operation of the heat pipe. To test the power capacity of the heat pipe, a power resistor was used to apply heat into the pipe and induce dry-out of the wick. After dry-out conditions were met, the heat pipe was returned back to steady-state saturation conditions.

Future work on the cryogenic heat pipe consists of constructing a toroidal heat pipe so that a coil of HTS wire can be tested. With a coil of HTS wire one can test the operation of the system by driving large amounts of current into the wire, in addition to using a wheatstone bridge to test for changes in HTS resistance. For final validation, it is proposed to use a thermal

vacuum chamber, to incorporate a sun and Earth heat source and include the radiator in the EMFF thermal system. One of the factors driving the design of the heat pipe that was shown in this paper was manufacturing of the wick and copper envelope. The performance of the heat pipe can be optimized by using different types of wicks, such as sintered metal fibers, and the mass of the pipe reduced by using a lightweight envelope, thus making the EMFF cryogenic thermal control system more viable for flight.

REFERENCES

- [1] Sakaguchi, Aya, "Micro-Electromagnetic Formation Flight of Satellite Systems," S.M. Thesis, Massachusetts Institute of Technology, SSL #20-07, June, 2007.
- [2] Kwon, Daniel W., and Miller, David W., "Electromagnetic Formation Flight of Satellite Arrays," S.M. Thesis, Massachusetts Institute of Technology, SSL #02-05, January 2005.
- [3] American superconductor, "Bi-2223 High Strength Wire," URL: <http://www.amsuper.com> [cited 2 February 2008].
- [4] Keiter, Douglas E., and Wilson, Kyle B., "Sunpower Cooling Solutions," Sunpower Inc., Athena, Ohio.
- [5] Beam, Jerry, Brennan Patrick J., and Bello, Mel, "Design and Performance of a Cryogenic Heat Pipe Experiment (CRYOHP)," AIAA 92-2867, AIAA 27th Thermophysics Conference, Nashville, TN, July 6-8, 1992.
- [6] Elias, Laila M., Kwon, Daniel W., Sedwick, Raymond J., and Miller, David W., "Electromagnetic Formation Flight Dynamics including Reaction Wheel Gyroscopic Stiffening Effects" Journal of Guidance, Control, and Dynamics, Vol. 30, No. 2, Mar-Apr. 2007.
- [7] Kwon, Daniel W. "Electromagnetic Formation Flight System Design," 6th IAA Symposium on Small Satellites for Earth Observation, IAA-B6-0602, Berlin, Germany, April 23-26, 2007.
- [8] Reay, David A., Kew, Peter A., "Heat Pipes," Elsevier, Boston, 5th Edition, 2006.
- [9] Mills, A.F., "Heat and Mass Transfer," Prentice Hall, New Jersey, 2nd Edition, 1999.
- [10] Chi, S.W., "Heat Pipe Theory and Practice: A Sourcebook," McGraw-Hill, 1976.
- [11] Peterson, George P., "An Introduction to Heat Pipes: Modeling, Testing, and Applications," John Wiley & Sons, Inc., New York, 1994.